Bifurcation of a dielectric elastomer balloon under pressurized inflation and electric actuation

Y.-X. Xie[a,b], J.-C. Liu[a,b], Y.B. Fu[a,c,]

[a] *Department of Mechanics, Tianjin University, Tianjin 300072, China*
[b] *Tianjin Key Laboratory of Modern Engineering Mechanics, Tianjin 300072, China*
[c] *Department of Mathematics, Keele University, ST5 5BG, U.K.*

Abstract

It is previously known that under inflation alone a spherical rubber membrane balloon may bifurcate into a pear shape when the tension in the membrane reaches a maximum, but the existence of such a maximum depends on the material model used: the maximum exists for the Ogden model, but does not exist for the neo-Hookean, Mooney-Rivlin or Gent model. This paper discusses how such a situation is changed when a pressurized dielectric elastomer balloon is subjected to additional electric actuation. A similar bifurcation condition is first deduced and then verified numerically by computing the bifurcated solutions explicitly. It is shown that when the material is an *ideal* dielectric elastomer, bifurcation into a pear shape is possible for all material models, and similar results are obtained when a typical non-ideal dielectric elastomer is considered. It is further shown that whenever a pear-shaped configuration is possible it has lower total energy than the co-existing spherical configuration.

Keywords: Dielectric elastomer, Bifurcation, Instability, Spherical balloons, Nonlinear elasticity

1. Introduction

Dielectric elastomers are now widely recognized as a high-tech engineering material that has a variety of applications, ranging from robotics where it is used as artificial muscles, to energy harvesting where it is used to convert mechanical energy into electricity. They have received a lot of attention since they were first reported (Patrick et al. (2007), Kofod (2008), Fox and Goulbourne (2008), Pelrine and Prahlad (2008)). A key question that is addressed by many recent studies is their shape bifurcation and its effect on the performance and reliability of structures/devices made from such soft materials; see, e.g., Plante and Dubowsky (2006), Bertoldi and Gei (2011), De Tommasi et al. (2013), Dorfmann and Ogden (2014a), and the references therein.

Email address: y.fu@keele.ac.uk (Y.B. Fu)

There are many types of configurations for the generators and actuators made from dielectric elastomers, and one of them is the spherical balloon shape (Soleimani and Menonn (2010), Artusi et al. (2011)). A procedure was presented by Ahmadi et al. (2011) for fabricating and testing a seamless spherical dielectric elastomer balloon. Various aspects of the uniform inflation problem, such as the so-called limiting-point instability, have been examined by Mockensturm and Goulbourne (2006), Zhu et al. (2010), He et al. (2011), Rudykh et al. (2012), Keplinger et al. (2012), and Dorfmann and Ogden (2014b). York et al. (2010) and De Tommasi et al. (2014) studied the hysteresis effects commonly exhibited in such structures.

Since a spherical balloon is an important configuration in the application of dielectric elastomers, it is also of interest to understand whether shape bifurcation will take place when it is subjected to the combined action of internal inflation and a voltage. When a membrane balloon is under internal inflation alone, it is well known that the spherical shape may bifurcate into a pear shape when the internal volume reaches a first critical value, and then return to a spherical shape at a second, higher critical value (Feodosev (1968), Haughton and Ogden (1978), Ericksen (1998)). Chen and Healey (1991) showed that the pear-shaped configuration must necessarily have lower energy than the co-existing spherical configuration, and they also derived some sufficient conditions under which the above bifurcation behavior actually occurs for a general material model. Fu and Xie (2014) analyzed the stability of the pear-shaped configuration itself with respect to further axi-symmetric perturbations, and showed that it is stable under mass or volume control but unstable under pressure control. The well-known bifurcation condition in the purely mechanical case was originally derived from the incremental theory of nonlinear elasticity, but it was shown in Fu and Xie (2014) that if attention is focused on axi-symmetric bifurcation modes then bifurcation can be detected by a simple shooting procedure based on the original governing equations. It is this latter method that will be employed in the present paper. Our main objective is to understand how adding electric actuation affects the appearance of the pear-shaped configurations. We first extend the bifurcation condition for the purely mechanical case in a straightforward manner, and then verify that the extended bifurcation condition is indeed valid by using the above-mentioned shooting procedure.

The remainder of this paper is organized as follows. Section 2 presents the governing equations for the axi-symmetric deformations of a dielectric elastomer spherical balloon. These equations are then solved in Section 3 to find pear-shaped configurations that may bifurcate from the spherical configuration, guided by the bifurcation condition that was extended from its counterpart in the purely mechanical case. The total energy is computed to demonstrate that whenever a pear-shaped configuration can exist it is preferred to the co-existing spherical configuration. We conclude the paper in Section 4 with a discussion of how electric actuation based on different

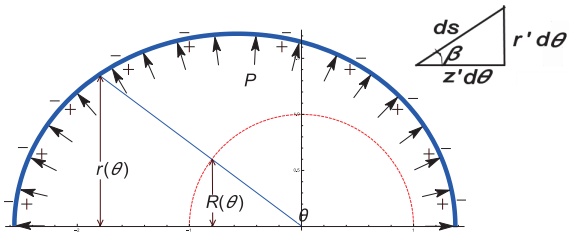

Figure 1: Undeformed and deformed configurations of a dielectric elastomer balloon under both pressurized inflation and electric actuation.

material models affects the appearance of the pear-shaped configurations.

2. Governing Equations

Figure 1 shows the upper half of a spherical balloon that is made of a dielectric elastomer material and is subjected to both internal inflation and electric actuation of the compliant electrodes attached to the inner and outer surfaces. Without loss of generality, the initial radius is assumed to be unity (which is equivalent to using the initial radius as the unit of length), and so the undeformed configuration Ω is described by

$$R(\theta) = \sin\theta, \quad Z(\theta) = 1 - \cos\theta, \quad 0 \le \theta \le \pi$$

in terms of cylindrical polar coordinates. We focus on axi-symmetric deformations (spherical or pear-shaped) described by

$$r = r(\theta), \quad z = z(\theta), \quad 0 \le \theta \le \pi,$$

where (r, θ, z) are cylindrical polar coordinates in the current configuration. The principal stretches are given by

$$\lambda_1 = \frac{r}{R}, \quad \lambda_2 = \sqrt{r'^2 + z'^2}, \quad \lambda_3 = \frac{h}{H},$$

where a prime denotes differentiation with respect to θ, and H and h are the thicknesses in the reference and deformed configurations, respectively.

According to Dorfmann and Ogden (2005), the total energy density function $\hat{W}$ of an incompressible dielectric elastomer can be assumed to be a function of the five invariants I_1, I_2, I_4, I_5, I_6 defined by

$$I_1 = \operatorname{tr} C, \quad I_2 = \operatorname{tr} C^{-1}, \quad I_4 = \boldsymbol{D}_l \cdot \boldsymbol{D}_l, \quad I_5 = \boldsymbol{D}_l \cdot C\boldsymbol{D}_l, \quad I_6 = \boldsymbol{D}_l \cdot C^2\boldsymbol{D}_l, \quad (1)$$

where C $(= F^T F)$ is the right Cauchy-Green deformation tensor, F is the deformation gradient, and $\boldsymbol{D}_l$ is the nominal electric displacement which is related to the true electric displacement $\boldsymbol{D}$ by $\boldsymbol{D}_l = F^{-1}\boldsymbol{D}$.

Following Dorfmann and Ogden (2014a), we shall consider the following simplest constitutive law that accounts for electro-elastic coupling:

$$\hat{W}(\lambda_1, \lambda_2) = W(\lambda_1, \lambda_2) + \frac{1}{2}\epsilon_0^{-1}(\xi I_4 + \eta I_5), \quad (2)$$

where $W(\lambda_1, \lambda_2)$ is the strain-energy density function of the elastomer per unit volume in the reference configuration, ϵ_0 is the vacuum permittivity, and ξ, η are two dimensionless material constants that characterize electroelastic coupling. The second term on the right hand side of (2) denotes the free energy associated with polarisation induced by the voltage. The above model reduces to that of an ideal dielectric elastomer when $\xi = 0$ and η is equal to ϵ_0 divided by the permittivity; see, e.g., Zhao and Suo (2007).

The electric field $\boldsymbol{E}$ is computed from $\boldsymbol{E} = F^{-T}\partial\hat{W}/\partial\boldsymbol{D}_l$, and is given by

$$\boldsymbol{E} = \epsilon_0^{-1}(\xi B^{-1}\boldsymbol{D} + \eta\boldsymbol{D}), \tag{3}$$

where $B = FF^T$. For the problem under consideration where a voltage ϕ is specified, we have

$$\boldsymbol{E} = \frac{\phi}{h}\boldsymbol{e}_3 = \frac{\phi}{H}\lambda_1\lambda_2\boldsymbol{e}_3,$$

where $\boldsymbol{e}_3$ denotes the unit vector normal to the membrane surface. It then follows that

$$\boldsymbol{D} = \epsilon\kappa(\lambda_1, \lambda_2)\boldsymbol{E}, \quad I_4 = \mu\Phi\lambda_1^4\lambda_2^4\epsilon\kappa^2(\lambda_1, \lambda_2), \quad I_5 = (\lambda_1\lambda_2)^{-2}I_4, \tag{4}$$

where

$$\epsilon = \epsilon_0/(\xi + \eta), \quad \Phi = \epsilon\phi^2/(\mu H^2), \quad \kappa(\lambda_1, \lambda_2) = (\xi + \eta)/(\xi\lambda_1^2\lambda_2^2 + \eta). \tag{5}$$

In the above expressions, the constants μ and ϵ denote the shear modulus and permittivity when there is no deformation, whereas the product $\epsilon\kappa(\lambda_1, \lambda_2)$ may be interpreted as the deformation-dependent permittivity corresponding to the simple model (2). It is then appropriate to impose the inequalities $0 < \xi + \eta \leq 1$. We observe that in the subsequent analysis the ground state permittivity ϵ will only appear through the non-dimensional parameter Φ, and ξ and η will always appear in the form ξ/η.

With the application of both a voltage ϕ and inner pressure P, the total free energy in the system takes the form

$$E = \int_\Omega \hat{W}(\lambda_1, \lambda_2)dV - Pv - \phi Q, \tag{6}$$

where v is the volume enclosed by the inner surface of the deformed balloon, and Q is the charge accumulated on each electrode. The Q and v may be calculated using the formulae

$$Q = \int_\Gamma \frac{\epsilon\kappa(\lambda_1, \lambda_2)\phi}{h}da = \int_0^\pi \frac{\epsilon\kappa(\lambda_1, \lambda_2)\phi}{h} \cdot 2\pi r\lambda_2 d\theta, \quad v = \int_0^\pi \pi r^2 z' d\theta,$$

where Γ denotes the current configuration of the inner surface. With the use of these expressions and introduction of a new *effective strain-energy function* $\tilde{W}$ defined by

$$\tilde{W} \equiv \mu^{-1}\hat{W}(\lambda_1, \lambda_2) - \Phi\kappa(\lambda_1, \lambda_2)\lambda_1^2\lambda_2^2, \tag{7}$$

equation (6) can be simplified to

$$E/(2\pi H\mu) = \int_0^\pi \mathcal{L}(\boldsymbol{u}, \boldsymbol{u}')d\theta, \tag{8}$$

where $\boldsymbol{u} = (r(\theta), z(\theta))$, and

$$\mathcal{L}(\boldsymbol{u}, \boldsymbol{u}') = \tilde{W}(\lambda_1, \lambda_2)\sin\theta - \frac{1}{2}\bar{P}r^2 z', \quad \bar{P} = P/(\mu H). \tag{9}$$

The associated Euler-Lagrange equation is

$$\frac{\partial \mathcal{L}}{\partial \boldsymbol{u}} - \left(\frac{\partial \mathcal{L}}{\partial \boldsymbol{u}'}\right)' = 0, \tag{10}$$

from which we obtain the equilibrium equations

$$\tilde{W}_1 - \bar{P}rz' - \left(\frac{\tilde{W}_2 r' \sin\theta}{\lambda_2}\right)' = 0, \tag{11}$$

and

$$\frac{\tilde{W}_2 z' \sin\theta}{\lambda_2} - \frac{\bar{P}r^2}{2} = 0. \tag{12}$$

With the use of the relations $r = \lambda_1 \sin\theta$, $r' = \lambda_2 \sin\beta$, $z' = \lambda_2 \cos\beta$, where β is the angle between the meridian and the z-axis (see Fig. 1), the equilibrium equations can be rewritten as a system of first-order ODEs:

$$\begin{aligned}
\lambda_1' &= \frac{\lambda_2 \sin\beta - \lambda_1 \cos\theta}{\sin\theta}, \\
\lambda_2' &= \frac{\csc\theta\left\{[\tilde{W}_1 - \lambda_2\tilde{W}_{12}]\sin\beta - \cos\theta[\tilde{W}_2 - \lambda_1\tilde{W}_{12}]\right\}}{\tilde{W}_{22}}, \\
\beta' &= \frac{\tilde{W}_1 \cos\beta \csc\theta - \lambda_1\lambda_2\bar{P}}{\tilde{W}_2},
\end{aligned} \tag{13}$$

where $\tilde{W}_1 = \partial\tilde{W}/\partial\lambda_1, \tilde{W}_{12} = \partial^2\tilde{W}/\partial\lambda_1\partial\lambda_2$, etc.

We first consider an ideal dielectric with its strain energy function described by the Ogden material model:

$$W(\lambda_1, \lambda_2) = \sum_{r=1}^{3} \frac{\mu_r}{\alpha_r}(\lambda_1^{\alpha_r} + \lambda_2^{\alpha_r} + (\lambda_1^{-1}\lambda_2^{-1})^{\alpha_r} - 3), \tag{14}$$

where the material constants, for an acrylic polymer, are given by $\alpha_1 = 1.3, \alpha_2 = 5.0, \alpha_3 = -2.0, \mu_1 = 1.491, \mu_2 = 0.003, \mu_3 = -0.024$, respectively, and W has been scaled by the ground state shear modulus. Other material models will be discussed in the final section.

When the deformed configuration is spherical, we have

$$\lambda_1 = \lambda_2 = \lambda, \quad \beta = \frac{\pi}{2} - \theta, \quad \bar{P} = \frac{2\tilde{W}_2(\lambda, \lambda)}{\lambda^2}. \tag{15}$$

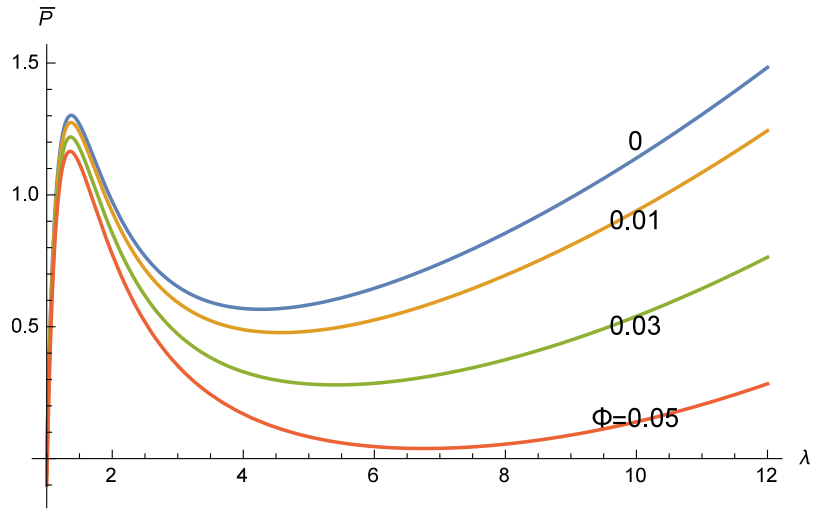

Figure 2: Variation of inflating pressure with respect to the principal stretch λ under fixed voltages in uniform inflation.

Figure 2 shows the inflating pressure versus the principal stretch λ under different fixed voltages when the material is an ideal dielectric. When Φ is small enough, each curve has a maximum and a minimum as in the purely mechanical case, but the electric voltage may significantly reduce the pressure minimum and hence increase the length of the descending branch. There exists a critical value of Φ below which the minimum does not exist at all (Zhu et al. (2010)).

3. Pear-shaped configuration and the associated energy

In the purely mechanical case, the bifurcation condition for the appearance of a pear-shaped configuration is given by

$$\frac{d}{d\lambda}\left(\frac{W_1(\lambda,\lambda)}{\lambda}\right)=0. \tag{16}$$

This condition was derived by Haughton and Ogden (1978) with the use of the incremental theory of nonlinear elasticity. Since the membrane tension (i.e. the stretching force per unit length of the membrane in the current configuration) is given by $\lambda W_1 h = \lambda W_1 H\lambda_3 = HW_1/\lambda$, the above bifurcation condition corresponds to the tension reaching a maximum.

When a voltage is applied, the expression $(9)_1$ shows that the dielectric elastomer can be viewed as a purely elastic material with a strain-energy function $\tilde{W}$. Thus, a natural extension of (16) is

$$\frac{d}{d\lambda}\left(\frac{\tilde{W}_1(\lambda,\lambda)}{\lambda}\right)=0. \tag{17}$$

We now demonstrate its validity by using the approach of Fu and Xie (2014) to find bifurcated solutions explicitly. Our illustrative calculations will be carried out for the case of an ideal dielectric elastomer.

When the Ogden material model (14) is used and the voltage is such that $\Phi = 0.01$, equation (17) has two roots given by

$$\lambda_{\rm cr1} = 1.7123, \quad \lambda_{\rm cr2} = 2.8711. \tag{18}$$

The corresponding (normalized) pressures can be obtained from the third equation in (13) and are given by

$$\bar{P}_{\rm cr1} = 1.1107, \quad \bar{P}_{\rm cr2} = 0.6179. \tag{19}$$

These two solutions correspond to the two points **S** and **E** in Figure 3. We now verify that pear-shaped configurations can only exist between these two points by integrating the system of equations (13) numerically.

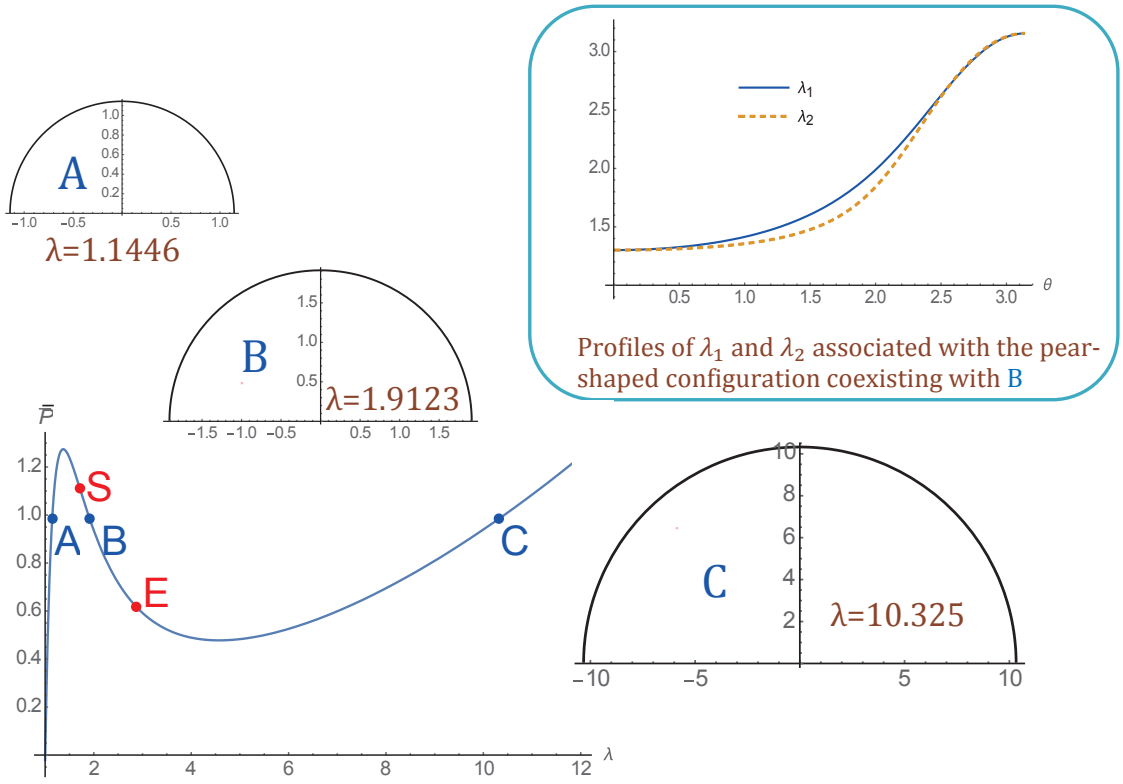

Figure 3: All possible solutions when $\bar{P} = 0.985$ and $\Phi = 0.01$. In addition to the three uniform solutions marked by points A, B and C, there is also a pear-shaped solution that can coexist with the uniform solution at point B. The framed inset depicts how λ_1 and λ_2 vary in the pear-shaped solution.

At the two poles of the balloon, we have

$$\lambda_1(0) = \lambda_2(0), \quad \lambda_1(\pi) = \lambda_2(\pi), \quad \beta(0) = \frac{\pi}{2},$$

$$\beta(\pi) = -\frac{\pi}{2}, \quad \lambda_1'(0) = \lambda_2'(0) = \beta''(0) = 0.$$

Since the right hand sides of the three equations in (13) cannot be evaluated at $\theta = 0, \pi$ directly, our numerical integration will be from $\theta = \delta$ to $\theta = \pi - \delta$, where δ is a sufficiently small parameter. Following Fu and Xie (2014), we may deduce the following series expansions:

$$\lambda_1(\delta) = \lambda_1(0) + \frac{1}{2}\lambda_1''(0)\delta^2 + O(\delta^4), \tag{20}$$

$$\lambda_2(\delta) = \lambda_1(0) + \frac{1}{2}\lambda_2''(0)\delta^2 + O(\delta^4), \tag{21}$$

$$\beta(\delta) = \frac{\pi}{2} + \beta'(0)\delta + \frac{1}{6}\beta'''(0)\delta^3 + O(\delta^5), \tag{22}$$

where at $\theta = 0$,

$$\lambda_1'' = \frac{(1-\beta'^2)(\tilde{W}_1 + 3\lambda_1\tilde{W}_{11} - \lambda_1\tilde{W}_{12}))}{8(\tilde{W}_{11})}, \tag{23}$$

$$\lambda_2'' = \frac{(1-\beta'^2)(3\tilde{W}_1 + \lambda_1\tilde{W}_{11} - 3\lambda_1\tilde{W}_{12})}{8(\tilde{W}_{11})}, \quad \beta' = -\frac{\lambda_1^2\bar{P}}{2\tilde{W}_1}, \tag{24}$$

$$\beta''' = \frac{\lambda_1\bar{P}(\lambda_1^4\bar{P}^2 - 4\tilde{W}_1^2)}{64\tilde{W}_{11}\tilde{W}_1^4}\{6\tilde{W}_1^2 + 3\lambda_1^2(\tilde{W}_{12}^2 - \tilde{W}_{11}^2) + \lambda_1\tilde{W}_1(\tilde{W}_{11} - 9\tilde{W}_{12})\}. \tag{25}$$

Similar expansions may be written down for $\lambda_1(\pi - \delta)$, $\lambda_2(\pi - \delta)$ and $\beta(\pi - \delta)$, and the expressions (23)–(25) are also valid at $\theta = \pi$. It is noted that in the above expansions only $\lambda_1(0)$ is unknown. The end condition $\beta(\pi) = -\pi/2$ may be replaced by

$$\frac{\pi}{2} + \beta(\pi - \delta) + \beta'(\pi - \delta)\delta = O(\delta^3). \tag{26}$$

We iterate on $\lambda_1(0)$ so that this end condition is satisfied. Typically we take $\delta = 0.01$ and set the iterations to stop when the left hand side of (26) becomes less than 10^{-5}.

Using the above shooting procedure and by scanning values of $\lambda_1(0)$ in a sufficiently large interval, we can find all possible solutions of (13) when the pressure lies between the two critical values given by (19). Our calculations confirm that pear-shaped configurations can only exist in this pressure interval, and when the two critical values are approached the pear-shaped solution coalesces into the spherical solution, exactly as we expected. For instance, when $\bar{P} = 0.985$, the three uniform solutions are first identified and the associated values of $\lambda_1(0)$ are given by

$$\lambda_1(0) = 1.1446, \quad 1.9123, \quad 10.325. \tag{27}$$

These solutions are marked by points **A**, **B** and **C** in Figure 3. Of course these solutions can also be determined trivially by solving the third equation in (15) alone.

Additionally, two other bifurcated solutions are also found, with $\lambda_1(0)$ given by

$$\lambda_1(0) = 1.3008, \quad 3.1556. \tag{28}$$

Each value corresponds to a pear-shaped configuration, but the two configurations are mirror images of each other in the sense that when $\lambda_1(0) = 1.3008$ we have $\lambda_1(\pi) = 3.1556$, whereas when $\lambda_1(0) = 3.1556$ we have $\lambda_1(\pi) = 1.3008$. Thus, we shall count these two bifurcated solutions as a single solution.

We next compare the energies associated with the co-existing spherical and pear-shaped configurations in order to show that the spherical configuration is unstable. The (normalized) free energies $E/(2\pi H\mu)$ of the system in the two configurations are denoted by $\bar{E}_u$ and $\bar{E}_b$, respectively, and can be computed with the aid of (8). The spherical configuration must necessarily be unstable if $\bar{E}_b - \bar{E}_u < 0$.

We select nine pressure values in the interval $\bar{P}_{\rm cr1}, \bar{P}_{\rm cr2}$, and calculate the associated energy difference $\bar{E}_b - \bar{E}_u$. The result are shown in Figure 4. It is clear that at each pressure value, the pear-shaped configuration has lower energy than the spherical configuration, which implies that the former is preferred when the system is on a state between points **S** and **E**.

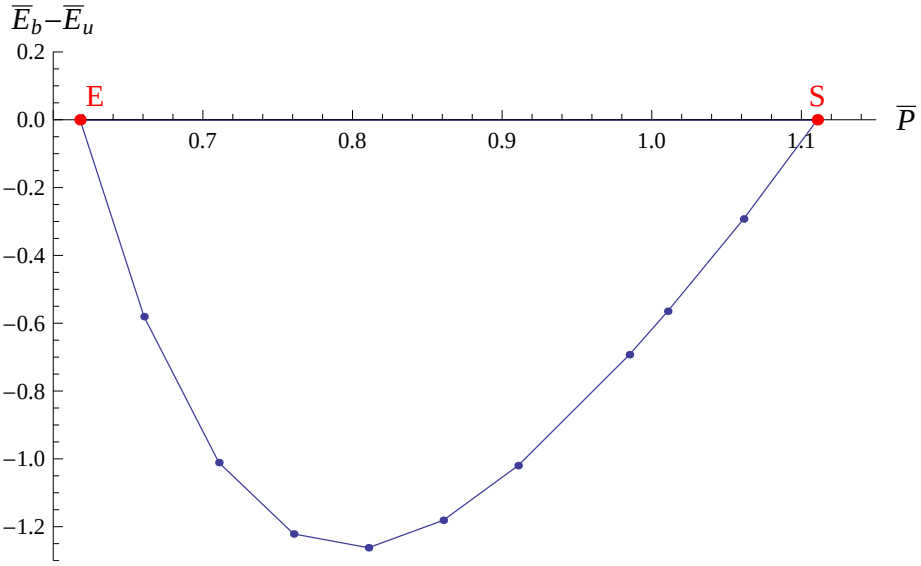

Figure 4: Difference in the total energy between pear-shaped and spherical configurations.

4. Dependence of bifurcation on the material models used

Having verified the validity of the bifurcation condition (17), we now take a closer look by rewriting it as

$$\frac{d}{d\lambda}\frac{W_1(\lambda,\lambda)}{\lambda} - \frac{2\lambda\Phi\eta(\xi+\eta)\left(\eta-3\lambda^4\xi\right)}{\left(\lambda^4\xi+\eta\right)^3} = 0. \tag{29}$$

For an ideal dielectric elastomer, the above condition reduces to

$$\frac{d}{d\lambda}\frac{W_1(\lambda,\lambda)}{\lambda} - 2\Phi\lambda = 0. \tag{30}$$

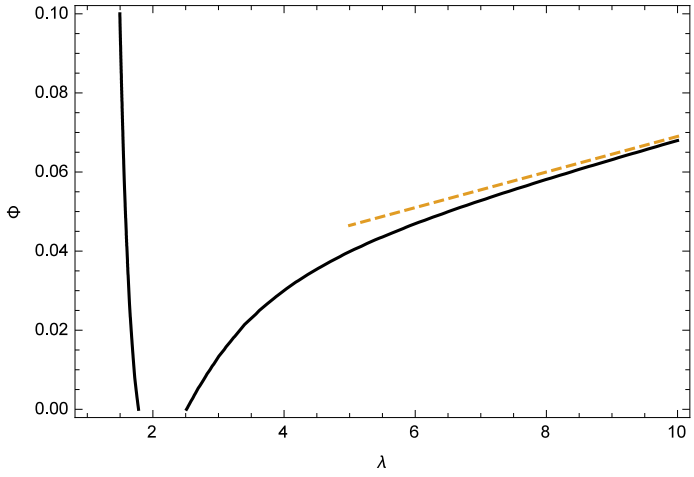

Figure 5: Solution of (30) (solid lines), and its asymptotic approximation $\Phi = 0.0045\lambda + 0.024$ for large λ (dashed line) when the mechanical part of the free-energy is given by the Ogden material model.

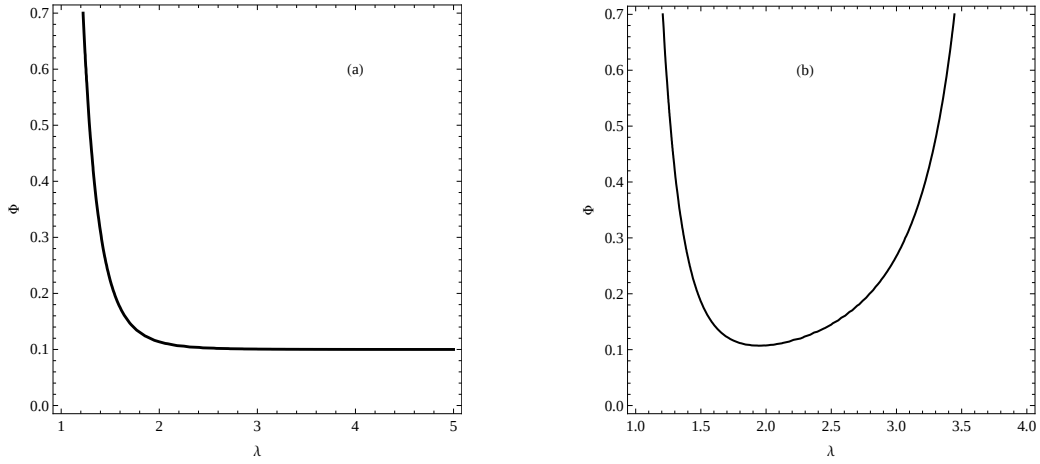

Figure 6: Solutions of (30) for (a) the Mooney-Rivlin material model with $\Gamma = 0.9$, and (b) the Gent material model with $J_m = 30$.

Since the second term is always negative, it follows that electric actuation makes it easier for a spherical balloon to bifurcate into a pear shape. Figure 5 shows more precisely how the addition of an electric field affects the bifurcation condition. In the purely mechanical case when $\Phi = 0$, there exist two bifurcation values of λ. When the smaller value is reached the spherical configuration will bifurcate into a pear-shaped configuration, and when the larger value is reached with continued inflation, the pear-shaped configuration will return to the spherical configuration. It can be seen from Figure 5 that when Φ is non-zero this pattern will persist although now the larger value of λ increases with respect to Φ and this dependence becomes linear when Φ becomes large.

The fact that the second term in (30) is always negative and is proportional to Φ

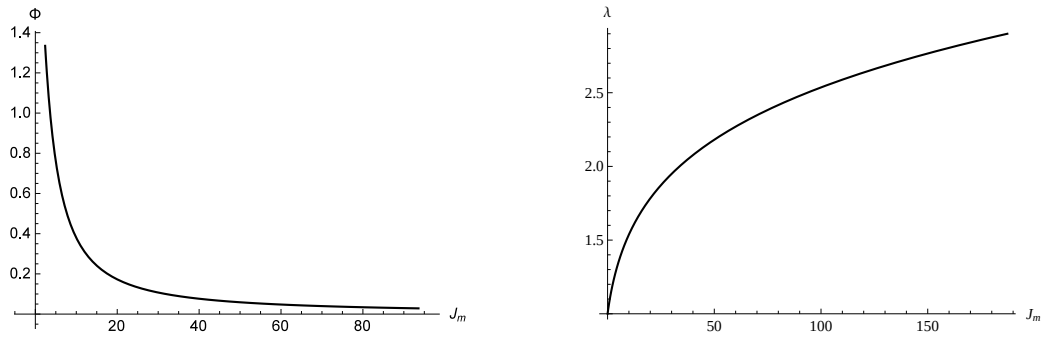

Figure 7: Dependence of (a) the minimum of Φ and (b) the associated value of λ in Figure 6(b) on J_m.

means that the bifurcation condition (30) always has a solution when Φ is sufficiently large. This is in sharp contrast with the purely mechanical case in which bifurcation is not possible for commonly used models such as the Mooney-Rivlin or Gent model for which the W is given by

$$W(\lambda_1, \lambda_2) = \frac{1}{2}\Gamma(\lambda_1^2 + \lambda_2^2 + \lambda_1^{-2}\lambda_2^{-2} - 3) + \frac{1}{2}(1-\Gamma)(\lambda_1^{-2} + \lambda_2^{-2} + \lambda_1^2\lambda_2^2 - 3), \quad (31)$$

and

$$W(\lambda_1, \lambda_2) = -\frac{1}{2}J_m \log\left(1 - \frac{\lambda_1^2 + \lambda_2^2 + \lambda_1^{-2}\lambda_2^{-2} - 3}{J_m}\right), \quad (32)$$

respectively, where Γ and J_m are material constants. In Figure 6(a, b) we have shown solutions of (30) for the Mooney-Rivlin and Gent material models, respectively. For the Mooney-Rivlin material, it can easily be deduce that as $\lambda \to \infty$, Φ tends to $1-\Gamma$, which means that bifurcation is possible only Φ is increased above the critical value $1-\Gamma$. For the neo-Hookean material model corresponding to $\Gamma = 1$, the asymptote becomes 0, which means that bifurcation into a pear-shaped configuration becomes possible as soon as Φ is non-zero. For the Gent material model, the minimum of Φ in Figure 6(b) depends on J_m. This dependence can be determined numerically and is shown in Figure 7. The neo-Hookean material model can be recovered by taking the limit $J_m \to \infty$, and Figure 7 again shows that the associated minimum of Φ is zero but it can only be attained in the limit $\lambda \to \infty$.

To illustrate how the bifurcation behavior depends on the model for the electric part of the total energy density function, Figure 8 depicts the solutions of (29) when $\xi/\eta = 0.001, 0.01, 0.03$. These solutions are qualitatively similar to their counterparts in Figure 6 in the sense that in each case bifurcation is only possible if Φ is larger than a certain threshold value that is dependent on ξ/η, the threshold value of Φ being an increasing function of ξ/η.

To summarize, we have demonstrated in this paper that when a pressurized dielectric membrane balloon is subjected to additional electric actuation, bifurcation into a pear-shaped configuration is expected to be the norm. More precisely, when the

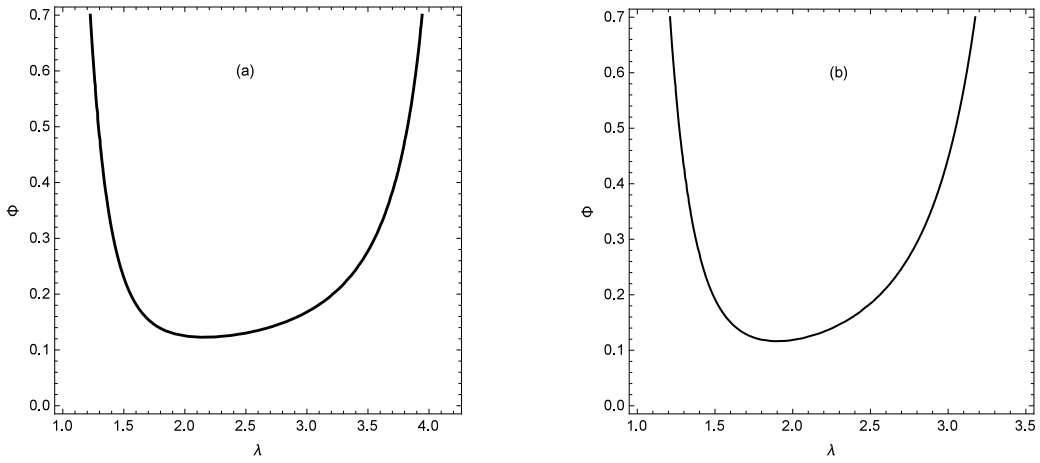

Figure 8: Solutions of the bifurcation condition (29) with $\xi/\eta = 0.001, 0.01, 0.03$ for (a) the Mooney-Rivlin material model with $\Gamma = 0.9$, and (b) the Gent material model with $J_m = 30$. The corresponding result to $\xi/\eta = 0$ is shown in Figure 6.

material is an ideal dielectric elastomer whose mechanical response is neo-Hookean or that of an Ogden material, then bifurcation becomes possible as soon as Φ is non-zero, whereas in the other cases bifurcation becomes possible only if Φ is larger than a certain threshold value that is dependent on material parameters. The formulae derived in this paper may be used to quantify the electric effects precisely.

Acknowledgements

This work is supported by the National Natural Science Foundation of China (grant nos 11172201 and 11372212).

References

Ahmadi, S., Gooyers, M., Soleimani, M. and Menon, C., 2013. "Fabrication and electromechanical examination of a spherical dielectric elastomer actuator. Smart Mater. Struct. 22, 115004.

Artusi, M., Potz, M., Aristizabal, J., Menon, C., Cocuzza, S., Debei, S., 2011. Electroactive elastomeric actuators for the implementation of a deformable spherical rover. IEEE-ASME Transactions on Mechatronics 16, 50-57.

Bertoldi, K., Gei, M., 2011. Instabilities in multilayered soft dielectrics. J. Mech. Phys. Solids 59, 18-42.

Chen, Y.-C., Healey, T.J., 1991. Bifurcation to pear-shaped equilibria of pressurized spherical membranes. International J. Non-Linear Mech. 26, 279-291.

De Tommasi, D., Puglisi, G., Zurlo, G., 2013. Inhomogeneous deformations and pull-in instability in electroactive polymeric films. Int. J. Non-Linear Mech. 57, 123-129.

De Tommasi, D., Puglisi, G., Zurlo, G., 2014. Hysteresis in electroactive polymers. Europ. J. of Mech. A/Solids. 48, 16-22.

Dorfmann, A. and Ogden, R. W., 2005. Nonlinear electroelasticity. Acta Mech. 174, 167-183.

Dorfmann, A. and Ogden R. W., 2014a. Instabilities of an electroelastic plate. Int. J. Eng. Sci. 77, 79-101.

Dorfmann, A. and Ogden R. W., 2014b. Nonlinear response of an electroelatic spherical shell. Int. J. Eng. Sci. 85, 163-174.

Ericksen, J. L., 1998. *Introduction to the thermodynamics of Solids*. Springer.

Feodosev, V.I., 1968. On equilbrium modes of a rubber spherical shell under internal pressure. PMM 32, 339-344.

Fox, J. W. and Goulbourne, N. C., 2008. On the dynamic electromechanical loading of dielectric elastomer membranes. J. Mech. Phys. Solids 56, 2669-2686.

Fu, Y.B., Xie, Y.X., 2014. Stability of pear-shaped configurations bifurcated from a pressurized spherical balloon. J. Mech. Phys. Solids 68, 33-44.

Kofod, G., 2008. The static actuation of dielectric elastomer actuators: how does pre-stretch improve actuation. J. Phys. D: Appl. Phys. 41, 215405.

Haughton, D. M., Ogden, R. W., 1978. On the incremental equations in non-linear elasticity: II. Bifurcation of pressurized spherical shells. J. Mech. Phys. Solids 26, 111-138.

He, X.Z., Yong, H.D., Zhou, Y.H., 2011. The characteristics and stability of a dielectric elastomer spherical shell with a thick wall. Smart Mate. Struct. 20, 055016.

Keplinger, C., Li, T.F., Baumgartner, R., Suo, Z.G., Bauer, S., 2012. Harnessing snap-through instability in soft dielectrics to achieve giant voltage-triggered deformation. Soft Matter 8, 285-288.

Mockensturm, E. M., Goulbourne, N., 2006. Dynamic response of dielectric elastomers. Int. J. Non-Linear Mech. 41, 38895.

Patrick, L., Gabor, K. and Silvain, M., 2007. Characterization of dielectric elastomer actuators based on a hyperelastic film model. Sensors and Actuators A: Physical 135, 748-757.

Pelrine, R., and Prahlad, H., 2008. Generator mode: devices and applications. In *Dielectric Elastomers as Electromechanical Transducers* (eds F. Carpi, D. De Rossi, R. Kornbluh, R. Pelrine, and P.-L. Sommer), Amsterdam: Elsevier, 146-155.

Plante, J. S., Dubowsky, S., 2006. Large-scale failure modes of dielectric elastomer actuators. Int. J. Solids Struct. 43, 7727-7751.

Rudykh, S., Bhattacharya, K., deBotton, G., 2012. Snap-through actuation of thick-wall electroactive balloons. Int. J. Non-Linear Mech. 47, 206-209.

Soleimani, M. and Menon, C., 2010. Preliminary investigation of a balloon-shape actuator based on electroactive elastomers. Smart Mater. Struct. 19, 047001.

York, A., Dunn, J., Seelecke, S., 2010. Experimental characterization of the hysteretic and rate-dependent electromechanical behavior of dielectric electro-active polymer actuators. Smart Mater. Struct. 19, 094014.

Zhao, X., Suo, Z, 2007. Method to analyze electromechanical stability of dielectric elastomers. Appl. Phys. Lett. 91, 061921.

Zhu, J., Cai, S.Q., Suo, Z.G., 2010. Nonlinear oscillation of a dielectric elastomer balloon. Poly. Int. 59, 378-383.